

Transport and modification processes of dense shelf water revealed by long-term moorings off Sakhalin in the Sea of Okhotsk

Yasushi Fukamachi,¹ Genta Mizuta,² Kay I. Ohshima,¹ Lynne D. Talley,³ Stephen C. Riser,⁴ and Masaaki Wakatsuchi^{1,5}

Received 14 April 2003; revised 26 April 2004; accepted 7 May 2004; published 15 July 2004.

[1] The region off the east coast of Sakhalin is thought of as an important pathway of dense shelf water (DSW) from its production region in the northwestern Okhotsk Sea to the southern Okhotsk Sea. From July 1998 to June 2000, the first long-term mooring experiment was carried out in this region to observe the southward flowing East Sakhalin Current (ESC) and DSW. Moored and associated hydrographic data show considerable modification of cold dense water via mixing with warm offshore water in the slope region off northern Sakhalin. Significant onshore eddy heat flux was observed at the northernmost mooring (54.9°N), which suggests the occurrence of baroclinic instability. The eddy heat flux was not significant farther south. At moorings along 53°N, cold anticyclonic eddies were identified that were consistent with isolated eddies seen in the hydrographic data. The three years of hydrographic data also showed large differences in extent and properties of DSW. Furthermore, the mooring data show that seasonal variability of DSW was quite different in the two years. The average DSW transport for $\sigma_\theta > 26.7$ evaluated using the moored data at 53°N for 1 year (1998–1999) was ~ 0.21 Sv ($= 10^6 \text{ m}^3 \text{ s}^{-1}$). This value is at the lower end of the previous indirect estimates. Along with the DSW modification, this transport estimate indicates that DSW was not only carried southward by the ESC but was spread offshore by eddies off northern

Sakhalin. **INDEX TERMS:** 4223 Oceanography: General: Descriptive and regional oceanography; 4243 Oceanography: General: Marginal and semiclosed seas; 4283 Oceanography: General: Water masses; **KEYWORDS:** Sea of Okhotsk, dense shelf water, mooring

Citation: Fukamachi, Y., G. Mizuta, K. I. Ohshima, L. D. Talley, S. C. Riser, and M. Wakatsuchi (2004), Transport and modification processes of dense shelf water revealed by long-term moorings off Sakhalin in the Sea of Okhotsk, *J. Geophys. Res.*, 109, C09S10, doi:10.1029/2003JC001906.

1. Introduction

[2] The Sea of Okhotsk (Figure 1) has a seasonal sea-ice cover despite its location at temperate latitudes. *Kitani* [1973] suggested that dense shelf water (DSW) with potential density up to $27.02\sigma_\theta$ is produced through sea-ice formation over the northwest shelf in this sea. Then this DSW is mixed with the water originating from the North Pacific and spreads southward. Eventually, the water affected by DSW exits to the North Pacific through the

Kuril Straits. Thus, DSW is the ventilation origin of the North Pacific Intermediate Water (NPIW), which spreads to the entire subtropical Pacific [*Alfultis and Martin*, 1987; *Talley*, 1991; *Warner et al.*, 1996; *Yasuda*, 1997].

[3] Because of this important impact on NPIW, the volume transport of DSW has been estimated in several recent studies. Using CFC data, *Wong et al.* [1998] estimated the volume transport in the range of $26.8\text{--}27.0\sigma_\theta$ to be larger than 0.6 Sv ($=10^6 \text{ m}^3 \text{ s}^{-1}$). Using Special Sensor Microwave/Imager (SSM/I) sea-ice data in 1990–1995 with dense water production models, *Martin et al.* [1998] estimated dense water production from 26.6 to $26.9\sigma_\theta$ to be $0.2\text{--}0.4$ Sv. Using hydrographic data on the northern shelves taken in 1995–1997, *Gladyshev et al.* [2000] estimated the volume transport in the range of $26.6\text{--}26.9\sigma_\theta$ to be 0.5 Sv in 1996 and 0.24 Sv in 1997. Using the historical bottle data and recent CTD data, *Gladyshev et al.* [2003] estimated the average DSW flux in the range of $26.7\text{--}27.0\sigma_\theta$ to be 0.6 Sv. Using a climatological data set in the Sea of Okhotsk averaged on isopycnal surfaces, *Itoh et al.* [2003] estimated the volume transport in the range of $26.75\text{--}27.05\sigma_\theta$ to be 0.67 Sv. *Shcherbina et al.* [2003,

¹Institute of Low Temperature Science, Hokkaido University, Sapporo, Japan.

²Graduate School of Environmental Earth Science, Hokkaido University, Sapporo, Japan.

³Scripps Institution of Oceanography, University of California, San Diego, La Jolla, California, USA.

⁴School of Oceanography, University of Washington, Seattle, Washington, USA.

⁵Also at Japan Science and Technology Corporation, Kawaguchi, Japan.

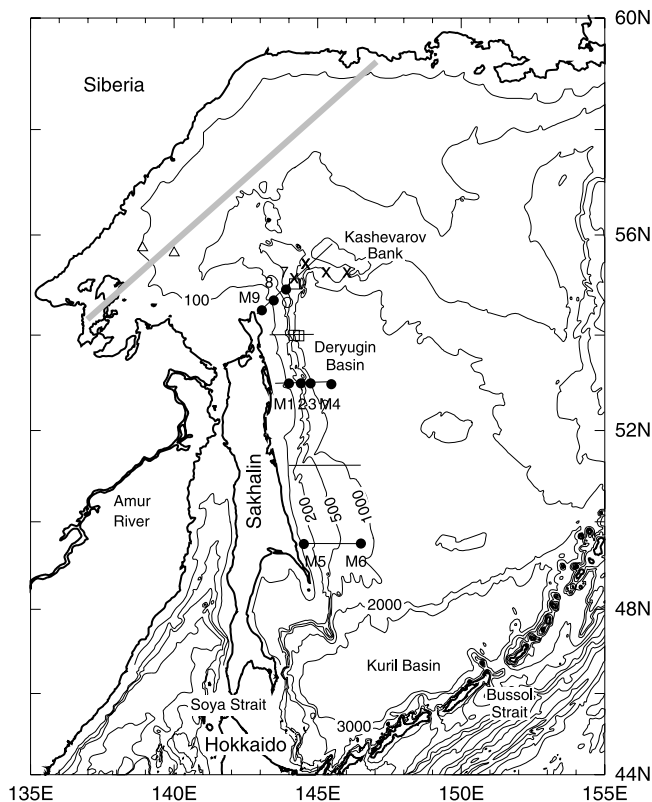


Figure 1. Bathymetry of the observation region based on the General Bathymetric Chart of the Oceans (GEBCO) data. Solid circles indicate locations of moorings. (For mooring M7, which was advected by strong currents, the solid and open circles denote locations of the deployment and recovery, respectively.) Crosses and squares indicate locations of CTD stations used to define the temperature of the offshore water and used as examples of the water affected by DSW, respectively (see Figure 2). The five lines off Sakhalin are CTD/XBT sections shown in Figures 3–5. Heat loss and the area of coastal polynya are estimated in the region enclosed by the shaded line and coastline over the northwest shelf (see Figure 13). Triangles on the northwest shelf denote locations of moorings discussed by *Shcherbina et al.* [2003, 2004a, 2004b].

2004b] report a range of 0.02–0.75 Sv of new DSW on the northwest shelf, upstream of the East Sakhalin Current (ESC), using moored current and water property measurements. We report herein the first estimate of DSW transport in the ESC based on current measurements combined with water-property data.

[4] The modification and expansion of DSW have been also investigated. Using hydrographic and oxygen isotope data from 1998–2000, *Yamamoto et al.* [2002] showed that the fraction of DSW in the intermediate water ($26.7\text{--}27.0\sigma_\theta$) off Sakhalin decreases southward from 50% at 54°N to $\leq 20\%$ to south of 51°N . Using CTD data from summer 1996, *Gladyshev et al.* [2003] showed that cold DSW in the range $26.7\text{--}9\sigma_\theta$ spreads offshore into Deryugin Basin north of 53°N as well as southward along Sakhalin. Owing to the lack of direct current measurement, however, the roles of eddies in these processes had never been examined.

[5] In 1998–2000, an intensive oceanographic study was conducted in the Sea of Okhotsk by Japanese, Russian, and U.S. institutions. This study revealed the existence of the ESC and its variability quantitatively well. This southward current had been regarded to carry DSW into the Kuril Basin. Using surface-drifter data, *Ohshima et al.* [2002] showed that the ESC is strongly controlled by bottom topography and confined to the region with bottom depths shallower than 1000 m. At about 48°N , the flow bifurcates; one branch of the current continues southward to the southern tip of Sakhalin and the other flows eastward as far as Bussol' Strait. Using the mooring data off the east coast of Sakhalin in 1998–2000, *Mizuta et al.* [2003] showed that the current extended from the surface to a depth of about 1000 m; its annual average transport was 6.7 Sv with a maximum of 12.3 Sv in February and a minimum of 1.2 Sv in October.

[6] Here the same long-term mooring data (velocity, temperature, and salinity) obtained in 1998–2000 are analyzed, focusing on water properties. Then transport and modification processes of DSW are investigated using these unique time series data. In addition, the hydrographic data collected during our three cruises off Sakhalin in 1998–2000 are also examined.

2. Data and Processing

[7] Mooring experiments were carried out in 1998–2000 at locations shown in Figure 1. The moorings were deployed from R/V *Professor Khromov* of Russian Far Eastern Regional Hydrometeorological Institute in shelf regions (M1, M5, M8, and M9), slope regions (M2, M3, and M7), and offshore regions (M4 and M6). Some of the moorings were deployed only during the period from July 1998 to September 1999 or from September 1999 to June 2000 (Table 1). All moorings were recovered successfully and most of the instruments yielded good data. Velocity data were obtained by both upward-looking acoustic Doppler current profilers (ADCPs) and current meters. Details of the velocity data are described by *Mizuta et al.* [2003]. In addition to the ADCPs and current meters, conductivity-temperature (CT) sensors (SeaBird SBE-37SM) and thermistors (Nichiyu-Giken NWT-SN and NWT-DN only for M6 at 740 m in 1999–2000) were deployed to monitor water properties.

[8] The pressure sensor (Rigo NEW-RMD) at the top instruments failed at moorings M2 and M4 in 1998–1999, so it was necessary to assume that the M2 and M4 instruments were always at their nominal depths. (The effect of this assumption is discussed in section 4.1.) At other moorings, variable depths of instruments are estimated from either the pressure sensor or ADCP at the top. Most instruments were moored in the depth range of 200–450 m in slope regions. This range roughly covers the layer of DSW, which has potential densities $\sim 26.7\text{--}27.1\sigma_\theta$.

[9] The CT sensors had an initial accuracy of 0.003 S/m and 0.002°C for conductivity and temperature, respectively. The post-cruise calibration showed no appreciable drift. The thermistor accuracy was 0.05°C . Temperature sensors on the current meter and ADCP had accuracies of 0.05°C and 0.4°C , respectively.

[10] In the shelf regions, except at M1 in 1999–2000, instruments were housed in a trawl resistant bottom mount

Table 1. Mooring Configurations^a

Period	Station	Latitude Longitude	Depth, m	Instrument	Nominal Depth, m
1998/7–1999/9	M1	53.0	100	ADCP	100
		144.0		CT	100
1999/9–2000/6	M1	53.0	100	CM	60
		144.0		CT	60
				TM	80
1998/7–1999/9	M2	53.0	480	CM	200/430
		144.4		CT	200/430
				TM	240 ^b /280 ^b /330/380
1999/9–2000/6	M2	53.0	480	CM	200/420
		144.4		CT	200/430
				TM	170/230/270/320 ^b /370 ^b
				PS	170
1998/7–1999/9	M3	53.0	970	ADCP	190
		144.8		CM	460/870
				CT	190/460
				TM	220 ^b /260/310/360/410
1998/7–1999/9	M4	53.0	1720	CM	200/480
		145.5		TM	280
		1999/9–2000/6		M4	53.0
145.5	CM		470		
	TM		210/260/360		
1998/7–1999/9	M5	49.5	130	ADCP	130
		144.5		CT	130
		1998/8–1999/9		M6	49.5
146.5	CM		480/750		
	CT		190		
	TM		280		
1999/9–2000/6	M6	49.5	780	ADCP	180
		146.5		CM	470/740
				TM	220/270/370 ^b /470/740
				PS	180
1999/9–2000/6	M7	54.9	480	ADCP	200
		143.9		CM	430
				CT	200/430
				TM	370 ^b
1999/9–2000/6	M8	54.7	110	ADCP	110
		143.5		CT	110
		1999/9–2000/6		M9	54.5
143.0	CT		90		

^aDates are given as yyyy/m. Acronyms CM, CT, TM, and PS denote current meter, conductivity-temperature sensor, thermistor, and pressure sensor. Those deployed at 240, 280, 320, and 370 m for M2 stopped in May and January 1999, April 2000, and December 1999, respectively.

^bThermistors stopped prematurely. Those deployed at 220 m for M3 and 370 m for M6 and M7 stopped in August 1999, February 2000, and October 1999, respectively.

(Flotation Technologies AL-200) to avoid damage due to fishing activities. The CT sensors in these mounts failed to measure conductivity accurately due to mud contamination into the conductivity cell. In the slope regions, some CT sensors occasionally had periods of anomalously low salinities (up to 1.363 from the expected values from the temperature-salinity (T-S) relation) not associated with low temperatures. It is likely that these anomalous values were also caused by the mud contamination, because Nakatsuka *et al.* [2002, Figure 3] showed that in this area, the cold temperature signal of the DSW coincided with high turbidity. Salinities during these periods are replaced with the values deduced from temperatures using the T-S relation during 10-day periods before and after these anomalous periods. The upper and lower sensors at M3 contained anomalous salinities for ~2% and 6% of all values, respectively. The lower sensor at M2 in 1999–2000 contained ~15% anomalous values. The upper and lower sensors at M7 contained <1% and ~2% anomalous values, respec-

tively. Despite these anomalous periods, salinities agreed reasonably well (<0.033) with those obtained by CTD during recovery at M2 and M3. In addition, salinity spikes with short timescales were removed.

[11] Mooring M7 was advected by strong currents and recovered about 29 km downstream (Figure 1). The depth data derived from the ADCP show significant changes twice. The estimated bottom depths are 480, 440, and 620 m during September–November, December–March, and March–June, respectively.

[12] Most of the mooring data were recorded at an hourly interval. A low-pass Lanczos-cosine filter with a cut-off frequency of 40 hours is applied to these data [Thompson, 1983]. These filtered data are used throughout this paper.

[13] The CTD data obtained off Sakhalin during the three cruises are also used. Instruments used were a SeaBird SBE 911 Plus in 1998, and a Neil Brown Mark III-B in 1999 and 2000. These data were corrected using the post-cruise calibration and water-sample measurements. Temperature

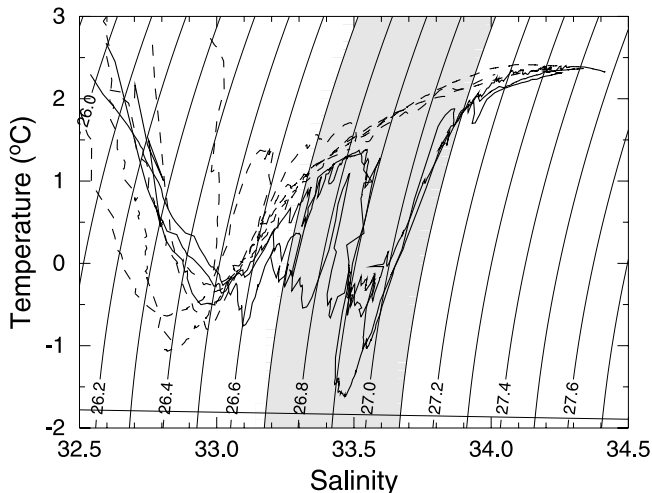


Figure 2. A T-S diagram to define properties of three water masses considered here. The thin curve near the bottom is the freezing point at the sea surface. Water that reaches this curve is regarded as the IDSW. Dashed curves are examples of offshore water drawn from the CTD data collected during the cruises in 1999 and 2000. (Station locations are indicated by crosses in Figure 1.) Thick curves are examples of water containing the MDSW drawn from the CTD data during the cruise in 1999. (Station locations are indicated by squares in Figure 1.) Near-surface data with temperature higher than 3°C or salinity lower than 32.5 are omitted.

data measured by expendable bathythermographs (XBTs) (Tsurumi Seiki) are also used.

3. Water Properties

[14] In the study region, we focus on three water masses in the intermediate layer (Figure 2). They are (1) the idealized dense shelf water (IDSW) with temperature at the freezing point, (2) warm and saline offshore water, and (3) the mixture of these two water masses, which is called modified dense shelf water (MDSW). The IDSW is produced in association with ice production mainly over the northwest shelf. The term IDSW is used only for the DSW at the freezing point, and this term is chosen because under ideal conditions the MDSW observed at moorings is converted to this quantity (see section 4.2). The offshore water originates in the North Pacific and is not influenced by DSW. The MDSW is characterized by low temperature and salinity in the range $26.7\text{--}27.1\sigma_\theta$ (shading in Figure 2).

3.1. CTD and XBT Data

[15] In the vertical sections of temperature and potential density drawn from the CTD and XBT data obtained during the three cruises (Figures 3–5), we focus on water with $\sigma_\theta > 26.7$ and negative temperature because such water is heavily influenced by the IDSW (Figure 2). These figures clearly illustrate the modification of water properties from north to south. At the northernmost section, the coldest water, with $T < -1.5^\circ\text{C}$, was in the density range $26.9 < \sigma_\theta < 27.0$ over the shelf (Figure 5a) and down along the continental slope (Figure 4a). At 53°N , the coldest water

was warmer and less dense, with $T < -0.5^\circ\text{C}$ and $26.7 < \sigma_\theta < 26.8$, over the outer shelf (Figures 3b and 4c), while water with $\sigma_\theta > 26.7$ and negative temperature did not occur over the slope except in the year 2000 (Figure 5c). Farther south, water with $\sigma_\theta > 26.7$ and negative temperature was almost entirely absent, except at 49.5°N in 1999 (Figure 4d). These downstream variations in water properties indicate that DSW mixed vigorously with warm offshore water as it flowed southward via the ESC. The patchy temperature distribution with many intrusions at the northern three sections are signs of such mixing. Using the hydrographic and oxygen isotope data, and the CFC data from the same cruises, Yamamoto *et al.* [2002, 2004] also showed this water modification off northern Sakhalin.

[16] Locations of cold DSW also changed from north to south. Cold DSW extended widely over the shelf and slope at the northernmost section (Figures 4a and 5a). The extent diminished toward the south and was mostly limited to being over the outer shelf or upper slope at 53°N . Cold DSW also existed in the form of detached patches off the slope (most notably in Figures 3b, 4a, and 4b). This may reflect offshore DSW transport by isolated eddies. Maps of potential temperature on isopycnal surfaces in the range $26.8\text{--}27.0\sigma_\theta$ (not shown) imply that DSW spread offshore in the region north of 53°N . These maps are consistent with similar maps based on the data collected during summer 1996 with better station coverage, shown in Figure 10 of Gladyshev *et al.* [2003]. These points will be further discussed in section 3.2.

[17] Figures 3–5 also indicate large temporal variability in water properties. A large patch of cold DSW off the slope was observed only in 1999 at 54°N (Figure 4b). Note that densities (temperatures) within this patch were higher (lower) than those in the smaller patches in the other 2 years. Water with negative temperatures dominated the layer $26.7 < \sigma_\theta < 26.8$ only in 1999 at 49.5°N (Figure 4d). Furthermore, the extent of cold DSW was wider in 1999 than in 2000 at the northernmost section. These results suggest that the largest DSW production among these three years occurred during winter 1998–1999 prior to the cruise in September 1999. Shcherbina *et al.* [2003] also reported variations in DSW properties on the northwest shelf that suggested more vigorous DSW production in 1998–1999 compared with 1999–2000.

3.2. Mooring Data

3.2.1. Slope and Offshore Regions

[18] To examine variability of cold DSW, depth-time plots of temperature and potential density in the slope region (Figure 6) and temperature in the offshore region (Figure 7) are examined at different moorings. They show different spatial and temporal variability. In general, cold DSW was seen continuously in certain seasons at M2 and M7, but was only intermittent at M3, M4, and M6, located farther offshore (most notably at M3).

[19] At M2 (Figures 6a and 6c), isopycnal depths showed clear seasonal variability with a rise in autumn and falling in winter. This variability is related to the geostrophic strength of the southward flowing ESC with a minimum in autumn and maximum in winter [Mizuta *et al.*, 2003]. Cold DSW was seen around the deepening $26.7\sigma_\theta$ isopycnal during winter. Denser cold DSW ($\sigma_\theta > 26.8$) was observed during

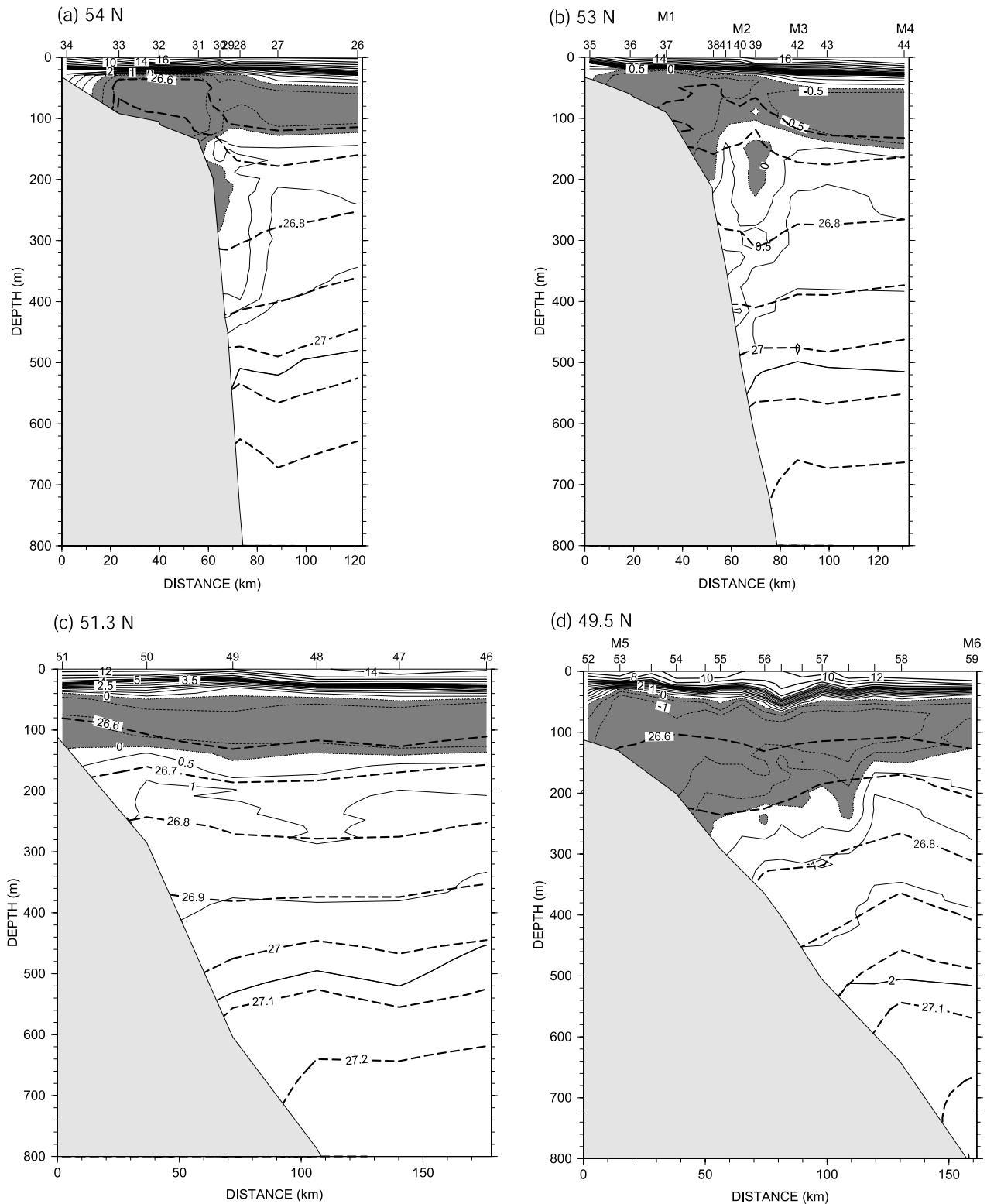


Figure 3. Vertical sections of temperature (solid and thin dashed contours for positive and negative values, respectively) and potential density (thick dashed contours only for $>26.6\sigma_\theta$) drawn from the CTD and XBT data obtained in late July and early August 1998. Four sections are along (a) 54°N , (b) 53°N , (c) 51.3°N , and (d) 49.5°N and are indicated by solid lines in Figure 1. Contour intervals are 0.5°C for temperature and $0.1\sigma_\theta$ for potential density. Regions of negative temperatures are shaded. Tick marks at the top with and without numbers correspond to CTD and XBT stations, respectively. Locations of moorings are also indicated at the top.

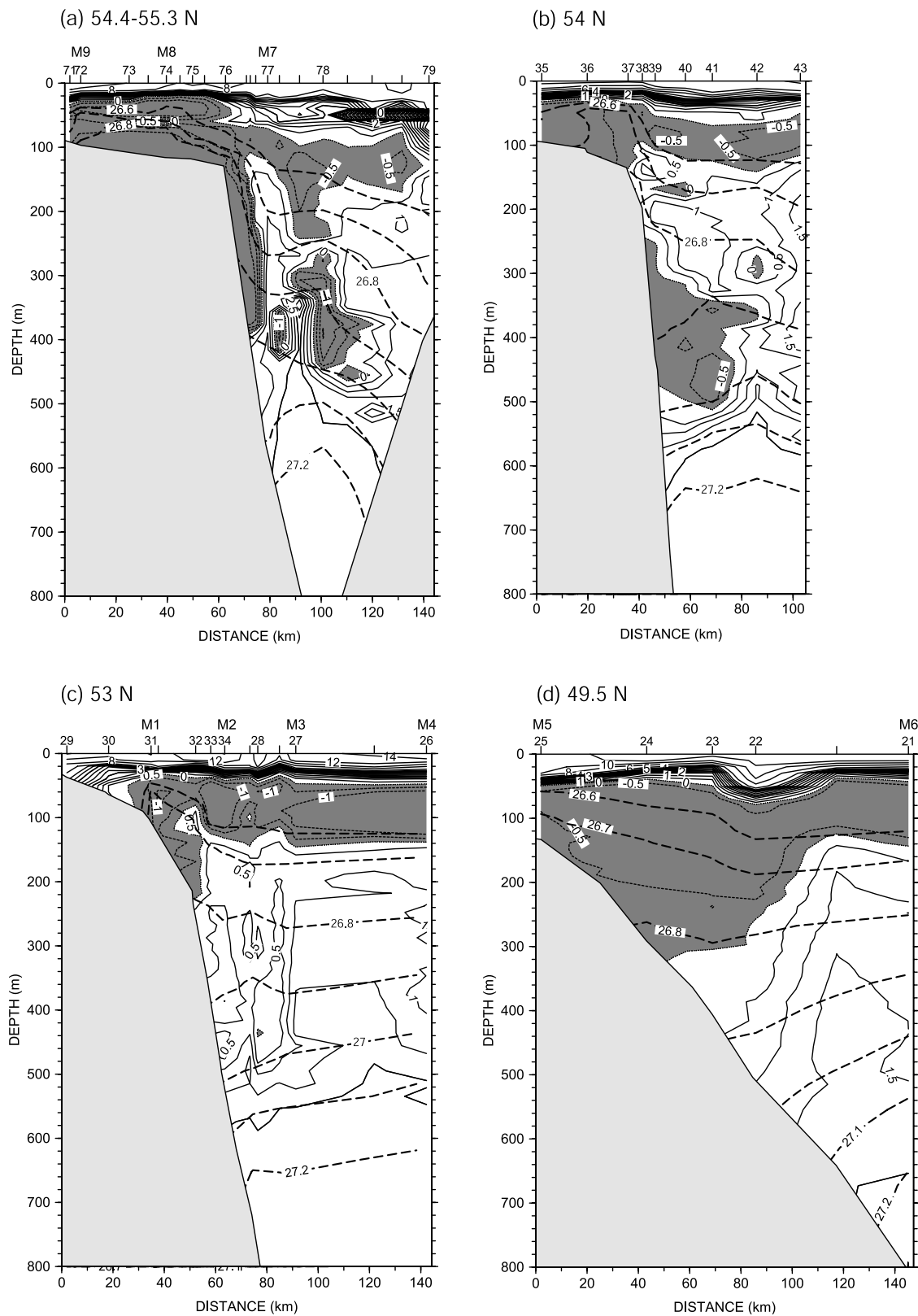


Figure 4. Similar to Figure 3, except for sections in September 1999. Four sections are (a) between 54.4°N and 55.3°N, and along (b) 54°N, (c) 53°N, and (d) 49.5°N.

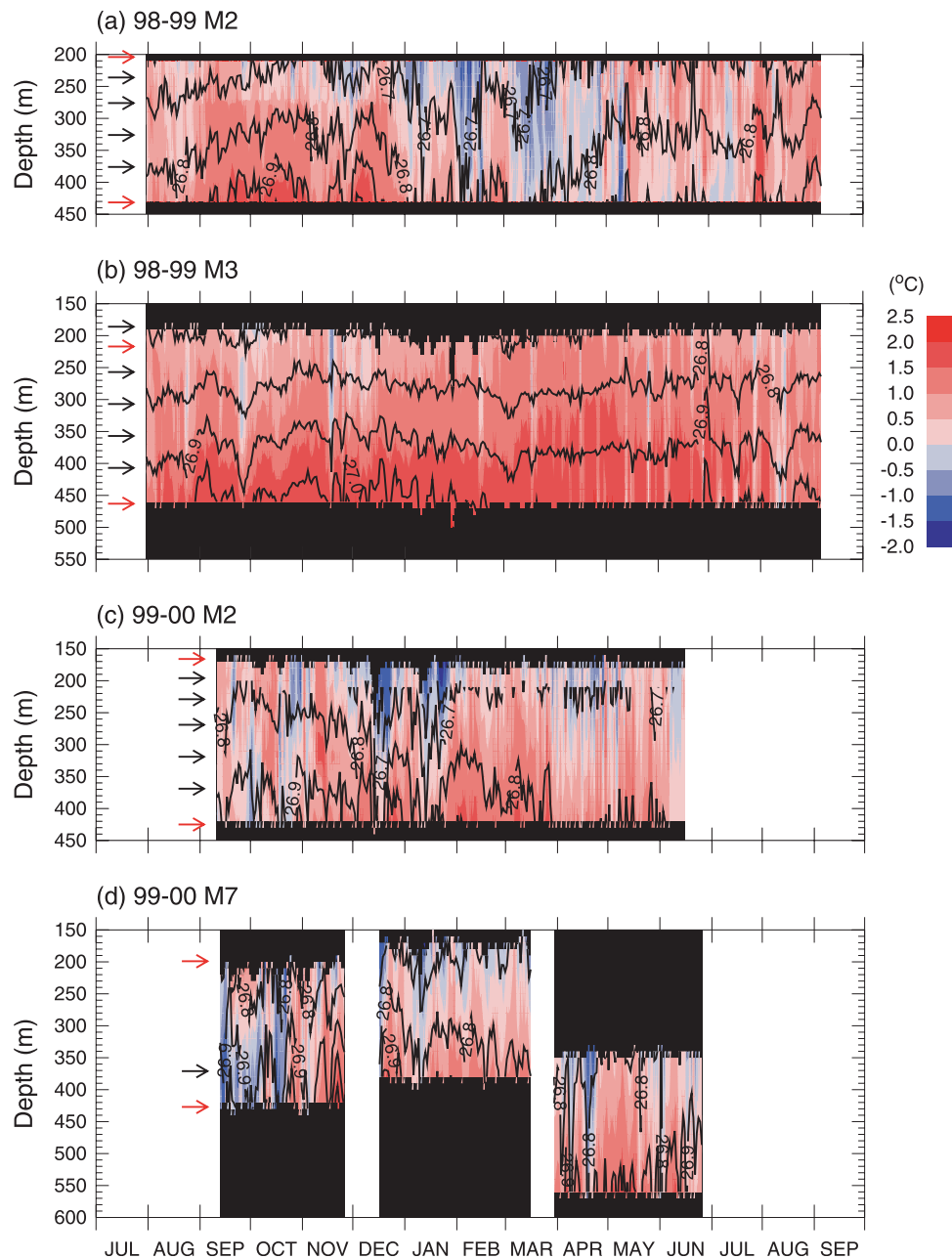


Figure 6. Depth-time plots of temperature and potential density in the slope regions at moorings (a) M2 and (b) M3 in 1998–1999, and (c) M2 and (d) M7 in 1999–2000. Temperature and potential density are displayed by color shading and contours, respectively. Intervals are 0.5°C for temperature and $0.1\sigma_{\theta}$ for potential density. Red and black arrows indicate nominal depths of the CT sensors and thermistors, respectively. Plotted data are interpolated between these instruments and subsampled at a daily interval. Note that values are not plotted in Figure 6d during the periods of depth changes, due to the movement of mooring M7.

Temperatures were usually positive for the entire mooring period except for short-term intermittent drops. Thus, cold DSW was present only during these events. The cold events in May–August were prominent over most of the observed depth range (see Figure 9 in section 3.2.3).

[21] At M7 (Figure 6d), isopycnal depths showed similar seasonal variability to that captured at M2. Cold DSW was most extensive in the density range $26.8 < \sigma_{\theta} < 27.0$ in September–November. In this period, temperatures were

lower at denser isopycnals, with average values of 0.23°C and 0.07°C at 26.8 and $26.9\sigma_{\theta}$, respectively. At M2, the decrease of temperature with depth was also present to a lesser extent, with average temperatures of 0.46°C and 0.43°C at 26.8 and $26.9\sigma_{\theta}$, respectively. Moreover, bottom-intensified flows were observed at both M7 and M2 in this period [Mizuta *et al.*, 2003]. The bottom-intensified flows were thus associated with cold DSW. The downstream increase in temperature from M7 to M2 was also seen in

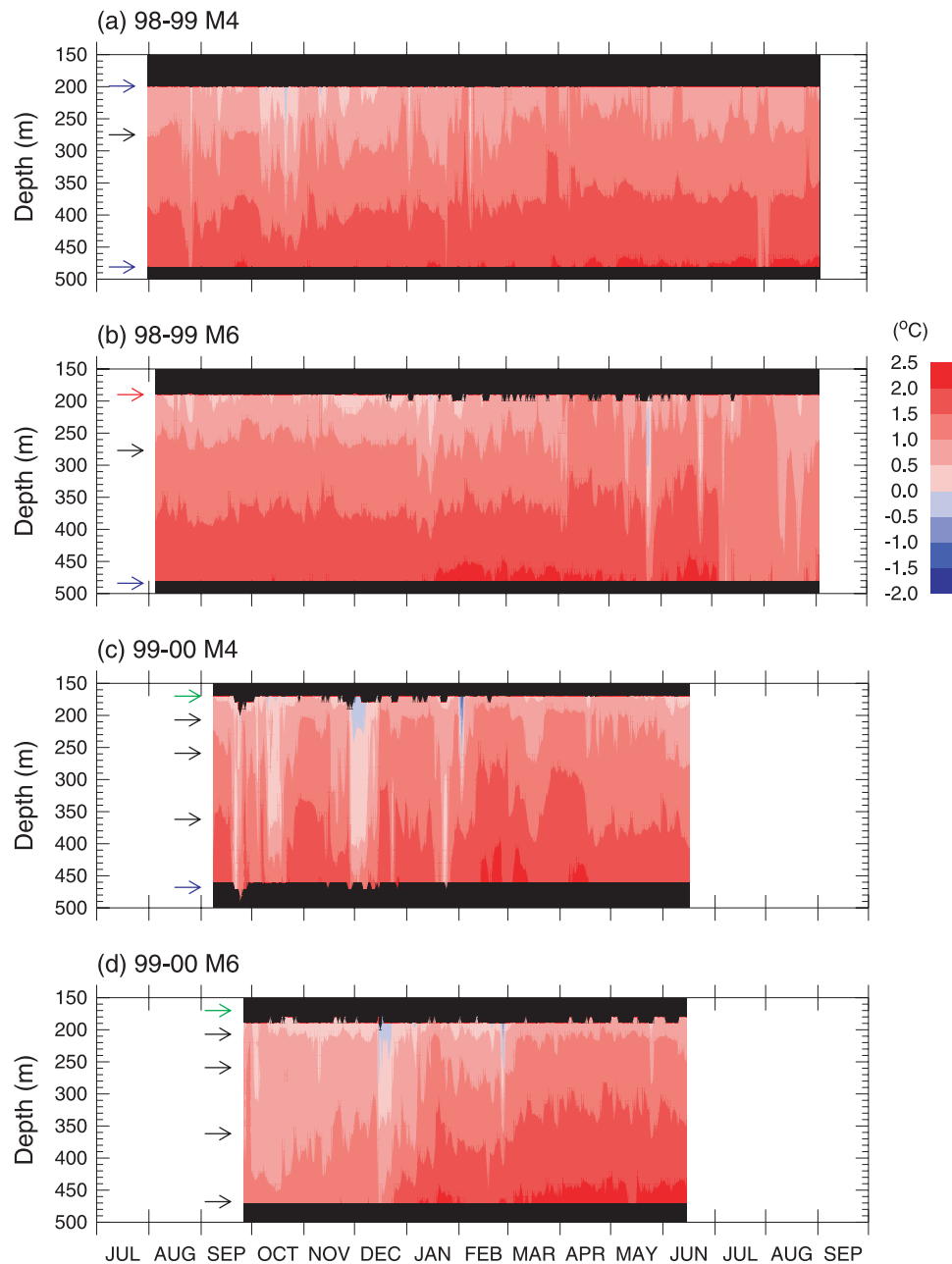


Figure 7. Similar to Figure 6, except for temperature in the offshore regions at (a) M4 and (b) M6 in 1998–1999 and at (c) M4 and (d) M6 in 1999–2000. Blue and green arrows indicate nominal depths of the current meters and ADCPs, respectively.

December–March. This temperature increase suggests that the cold water at M7 was considerably modified through mixing with the surrounding warmer water as it flowed downstream to M2 over a distance of ~ 220 km.

[22] At M4 in 1998–1999 (Figures 7a), the temperature drops seen at M3 (Figure 6b), which was located 48 km away, were nearly absent. From September 1999 to January 2000 (Figure 7c), however, relatively cold DSW was seen during short-term events. These cold events were prominent over most of the observed depth range. At M6 (Figures 7b and 7d), cold DSW was also seen only during short-term events. Note that temperatures at ~ 470 m were $\sim 1^\circ\text{C}$ lower in July–December 1999 than those in other periods. These

data at both M4 and M6 are consistent with the low temperatures seen at M2 below ~ 320 m (Figure 6c). This suggests that cold temperatures that occur over the slope can extend offshore and downstream.

3.2.2. Shelf Regions

[23] The CTD/XBT sections shown in Figures 4a and 5a clearly indicate the presence of cold DSW around moorings M8 and M9. Unfortunately, the conductivity sensors failed at these sites, so that no time series of DSW properties are available. At M1 in 1999–2000 (Figure 8c), potential density did not reach $26.7\sigma_\theta$ (upper dashed line) even during winter when temperatures were nearly at the freezing point. High densities close to $26.7\sigma_\theta$ were observed only in

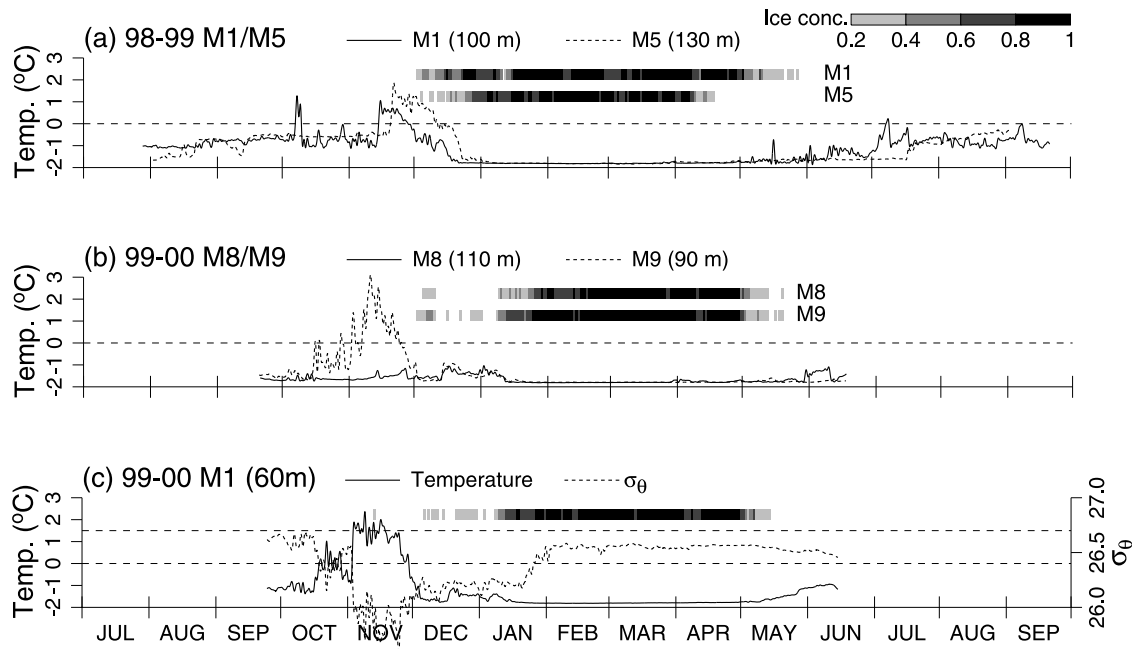


Figure 8. Temperature time series in the shelf regions at (a) M1 (solid curve) and M5 (dashed curve) in 1998–1999, and (b) M8 (solid curve) and M9 (dashed curve) in 1999–2000. (c) Temperature (solid curve) and potential density (dashed curve) time series at M1 in 1999–2000. Owing to the anomalous salinities from the CT sensors deployed at the bottom, the potential density time series is plotted only at M1 in 1999–2000, where the CT sensor was moored ~ 40 m above the bottom. These data are subsampled at a daily interval. Also, the daily sea-ice concentration derived from SSM/I data at the closest grid point from each mooring is displayed by the shading scale.

early fall. This is consistent with the presence of the cold dense water around M1 in the CTD/XBT section shown in Figure 4c. Since this section shows the presence of water with $\sigma_{\theta} > 26.7$ below 60 m, it is likely that the CT sensor moored at 60 m barely missed this dense water.

[24] There was clear seasonal variability in temperature except at M8 (Figure 8). Temperatures were negative throughout the deployment period except during fall. The positive temperatures during fall were caused by deepening of the surface mixed layer after the onset of the northwesterly monsoon. Note that this temperature increase was absent at M8, which was located only 33 km offshore of M9. The absence of this warm signal was likely due to the fact that the region around M8 was dominated by cold DSW during fall 1999. This is suggested by the CTD/XBT section shown in Figure 4a. Temperatures were nearly at the freezing point during late winter and early spring when sea-ice concentration was high.

3.2.3. Eddy components

[25] The remarkable intermittent temperature drops seen at M3 in the latter half of the mooring period (Figure 6b) are closely examined in Figure 9 using eddy components of temperature and velocity at 460 m. Salinity time series (not shown) indicate that these temperature drops corresponded to salinity drops. These temperature drops were usually associated with anticlockwise velocity evolution from the onshore to the along-isobath direction (roughly southward) and then to the offshore direction. The phenomena are consistent with cold anticyclonic eddies passing west of M3. On the basis of the duration of temperature drops and the mean along-isobath speed, scales of these eddies are

roughly estimated as 6–22 km. The size of a detached cold patch between M2 and M3 seen in Figure 3b is within this range. This cold patch and the similar features seen in Figures 4a and 4b suggest the transport of cold DSW by isolated eddies. The similar temperature drops seen at 470 m of M4 in December 1999 and January 2000 (Figure 7c) corresponded to the velocity evolution consistent with anticyclonic eddies passing east of M4.

[26] Since the maps of potential temperature on isopycnal surfaces suggest that DSW spread offshore in the region north of 53°N , eddy heat flux in the direction normal to isobaths is evaluated at the lower instruments of each mooring (Table 2). In most cases, values are negative, indicating the onshore eddy heat flux. The largest onshore heat flux occurred at M7. A good correlation between negative eddy temperatures and offshore eddy speeds during cold events resulted in large negative eddy heat flux, especially during spring 2000 (Figure 10). This suggests the occurrence of baroclinic instability associated with DSW near M7. At other moorings farther away from the DSW source region, onshore eddy heat flux was not significant. Rather, isolated cold eddies were merely advected southward at M3 and M4 (Figure 9). Thus, significant eddy heat flux is confined to the region off the northern tip of Sakhalin.

4. DSW Transport

4.1. MDSW

[27] Here the MDSW transport per unit horizontal length is calculated at the moorings in the slope regions. MDSW is defined here as water with $\sigma_{\theta} > 26.7$ and temperature lower

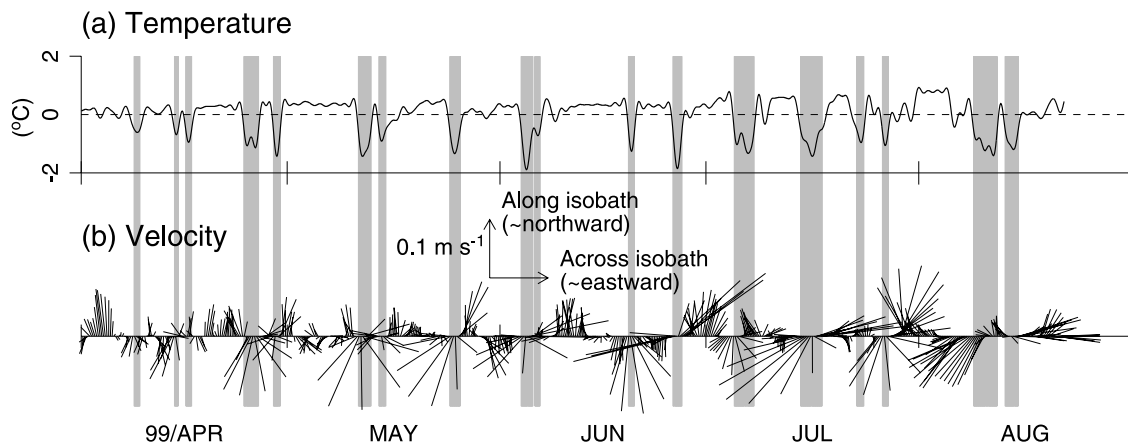


Figure 9. Time series of eddy (a) temperature and (b) velocity at 460 m of M3 in April–August 1999. Eddy components are derived by taking the difference between the data after the application of the low-pass filter and their 30-day running mean filtered ones. Velocity components are subsampled every 6 hours and shown in the rotated coordinates with respect to the isobath. Periods with low eddy temperatures ($< -0.5^{\circ}\text{C}$) are shaded.

than the average of four offshore-water values (evaluated in every $0.05\sigma_{\theta}$ bin) indicated by dashed curves in Figure 2. This transport is calculated as follows. First, the potential density, temperature, and current speed data are linearly interpolated to every 10 m between the sensors. For potential density, values from the upper and lower CT sensors (around 200 and 450 m) are used. For current speed, values from the upper and lower current meters are used at M2; at M3 and M7 the value from the lowest bin measured by the ADCP is used instead of that from the upper current meter. The direction of transport is taken as southward except for M7 in September–November at 20° anti-clockwise of south, which follows the bottom contours at the deployment location. For temperature, several values from the CT sensors and thermistors are used, except at M7, where only two or three values were observed due to instrument failures. (See Table 1 and Figures 6 and 7 for numbers and moored depths of these instruments.) Then, 10-m high interpolated cells that satisfy the MDSW definition were selected and their current speeds were summed to yield the MDSW volume transport per unit horizontal length. At M2 and M7, the depth range between the deepest interpolated cell and ocean bottom was included in this estimate, assuming that the current speed and water properties were uniform in this range and equal to those in the deepest cell measured.

Table 2. Eddy Heat Flux Normal to Isobath^a

Site	Period	Depth, m	Heat Flux, kW m^{-2}
M2	1998/8–1999/8	430	-5.10
	1999/9–2000/6	420	0.70
M3	1998/8–1999/8	460	-1.93
	1999/9–2000/6	470	3.38
M4	1998/8–1999/8	480	-1.05
	1999/9–2000/6	470	3.38
M6	1998/8–1999/4	480	-0.19
	1999/10–2000/5	470	-0.31
M7	1999/9–11	430	-19.00
	2000/1–2	390	-1.64
	2000/4–6	570	-44.88

^aDates are given as yyyy/m. A positive value indicates heat flux in roughly offshore direction. The correlation coefficient between eddy speed and temperature exceeds -0.5 only at M7 in April–June 2000.

[28] To evaluate the effect on the transport estimate of assuming that all the instruments at M2 in 1998–1999 were at their nominal depths, data from M2 in 1999–2000, which had an operating pressure sensor, are examined. The average depth change of the upper CT sensor in 1999–2000 was about 6 m, resulting in overestimation of the transport by $\sim 2\%$ if a constant depth was assumed. We conclude that this assumption does not affect transport estimate significantly.

[29] At M2 in 1998–1999 (Figure 11a), the transport was minimum and even northward in early fall. It increased through fall in winter, and then decreased in summer. Most of the transport was confined in the lower density bins ($\sigma_{\theta} < 26.8$) in January–April. On the other hand, the contributions from the higher-density bins were significant in November–December and May–August. It is likely that the signals in November–December and May–August corresponded to the DSW formation during the winter of 1997–

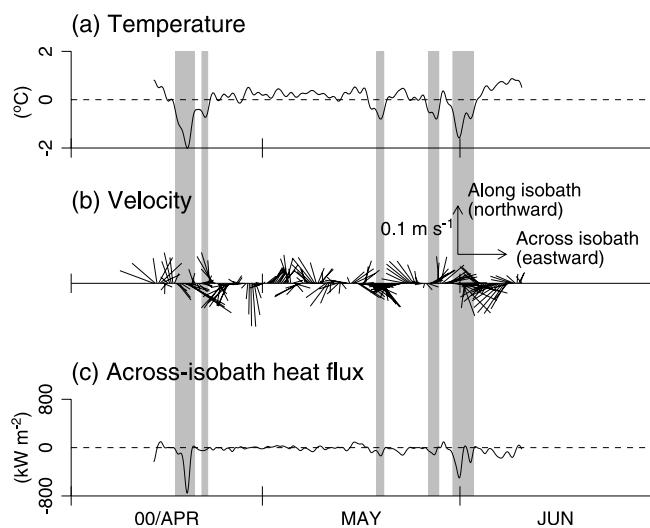


Figure 10. Similar to Figure 9, except for time series of eddy (a) temperature, (b) velocity, and (c) across-isobath heat flux at 570 m on M7 in April–June 2000.

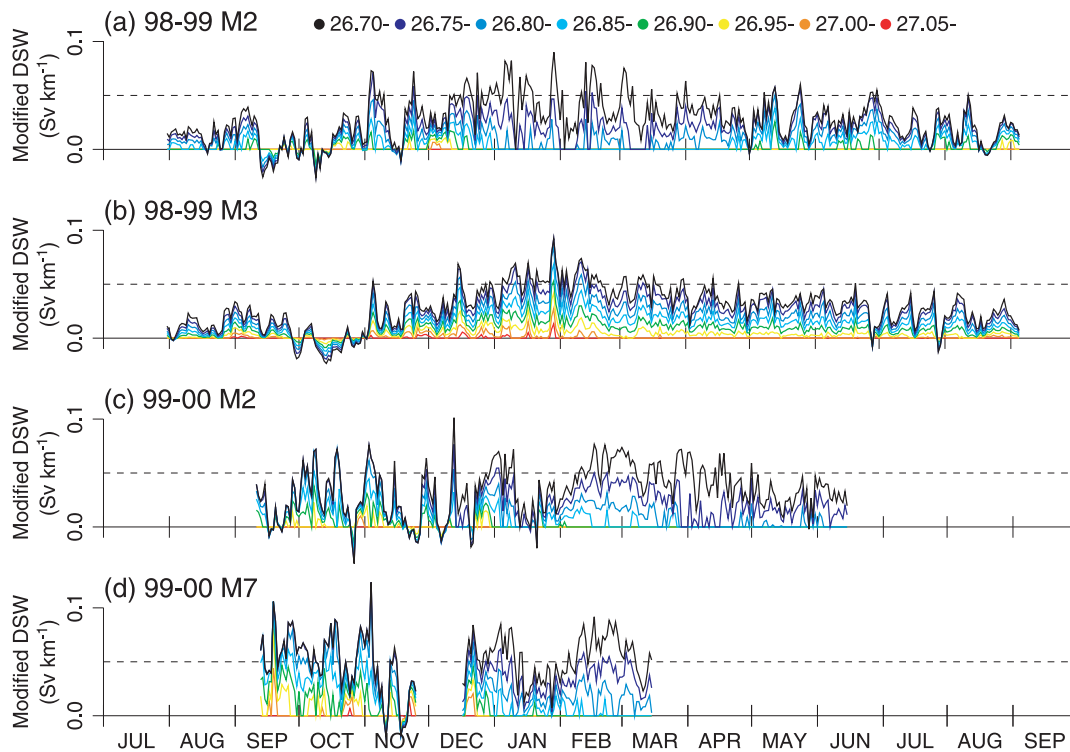


Figure 11. Time series of the MDSW transport per unit horizontal length (Sv km^{-1}) at the moorings in the slope regions. Distances between adjacent curves correspond to transport in $0.05\sigma_\theta$ bins, and the uppermost curve indicates the total transport for $\sigma_\theta > 26.7$. Data are plotted at a daily interval. Note that the transport was not shown from March to June for M7 because the range covered by the instruments was quite different from those in the two earlier periods.

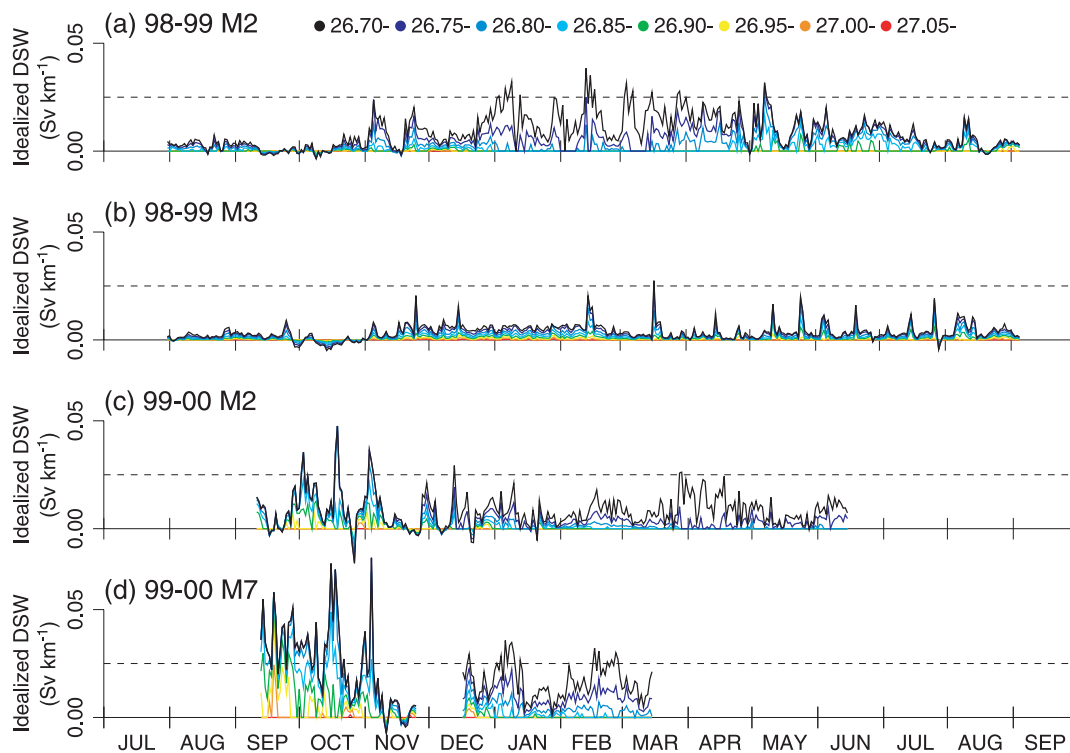


Figure 12. Similar to Figure 11, except for the IDSW. Note that the vertical scale is expanded from that in Figure 11 to show small values more clearly.

Table 3. Total, Modified, and Idealized DSW Transports Per Unit Horizontal Length ($\times 10^{-2}$ Sv km^{-1})^a

	M2		M3	M7	
	1998/8–1999/8	1999/9–2000/6	1998/8–1999/8	1999/9–11	1999/12–2000/3
Total	3.39	3.95	3.08	5.31	6.51
MDSW	2.75	3.42	2.86	5.00	5.38
IDSW	0.89	0.84	0.36	2.45	1.68
	(0.31)	(0.30)	(0.22)	(2.27)	(0.44)

^aDates are given as yyyy/m. Total transport is calculated regardless of water properties. The IDSW transport with $\sigma_\theta > 26.8$ is shown in parentheses.

1998 and 1998–1999, respectively. At M3 (Figure 11b), the net MDSW transport showed seasonal variability similar to that at M2. However, the contributions from density bins between 26.7 and 26.95 σ_θ were comparable throughout the mooring period. At M2, the seasonal variability of the transport differed between 1998–1999 and 1999–2000. The transport was relatively large in September–November 1999 (Figure 11c). In addition, the higher-density bins ($\sigma_\theta > 26.8$) occupied roughly half of the total transport in these months. The transport was also relatively large in February–March 2000. Unlike the previous year, the contributions from the larger density bins remained small even after April, due to the low densities then. At M7 (Figure 11d), variability was similar to that at M2 downstream. In fall, however, the transport was larger at M7. This is due to the larger flow speed at M7 than at M2 (see Tables 3 and 4 in section 4.2) and modification of water properties in between. The former implies that the flow field is more divergent at M2 than at M7 and/or that M7 was located closer to the core of the flow than M2.

[30] At all the moorings, seasonal variability of the MDSW transport was mainly due to total transport variability regardless of water properties. This is because the MDSW definition used here is not very strict and most of the total transport satisfies the MDSW definition (see Table 3 in section 4.2). At moorings M2 and M7, however, there were considerable differences in these two values due to deepening of the 26.7 σ_θ isopycnal during winter (see Figures 6a, 6c, and 6d).

4.2. IDSW

[31] Here the IDSW transport is derived because it is a more meaningful quantity directly related to sea-ice formation. It is derived by multiplying the mixing ratio of the IDSW to the MDSW transport shown in Figure 11. The mixing ratio is evaluated using the IDSW and offshore water as two end-members (Figure 2) and assuming isopycnal mixing. This evaluation is carried out based on temperature because there are several temperature measurements (except at M7) in this depth range (Figure 6). Specifically, the mixing ratio R is calculated using the following equation:

$$R = (T_O - T_M)/(T_O - T_I). \quad (1)$$

In equation (1), T_O is the average offshore temperature calculated from the four CTD profiles indicated by dashed curves in Figure 2, T_M is temperature in the interpolated 10-m-high cell derived from the mooring data, and T_I is the

IDSW temperature that is assumed to be uniform at -1.8°C . The value of T_O is evaluated in 0.05 σ_θ bins, and the value in the observed density bin of T_M is used in equation (1).

[32] Unlike the MDSW (Figures 11a and 11b), the IDSW transport was quite different between M2 and M3 in 1998–1999 (Figures 12a and 12b). The value was larger at M2 than at M3. This suggests that the core of IDSW was confined within a narrow zonal region at 53°N in 1998–1999. The IDSW transport at M3 occurred rather continuously in November–February and intermittently during temperature drops in April–August (Figure 9). The difference between M2 and M7 was larger than that for the MDSW (Figures 12c and 12d). This reflected the higher values of the IDSW mixing ratio at M7, because M7 was located closer to the IDSW source region and subject to less property modification. Since sea-ice production usually starts in November and becomes maximum in January (see Figure 13 in section 5), the IDSW seen in fall to early winter was formed in the previous winter. In fact, the DSW that formed in the previous winter was also observed during fall 1999 even farther north at the eastern mooring over the northwest shelf (see Figure 1 for its location) [*Shcherbina et al.*, 2003, 2004a]. Thus these data indicate that the outflow of DSW can occur in fall as well as in spring and summer. The derived IDSW transport at M2 clearly shows that seasonal variability was quite different between 1998–1999 and 1999–2000 (Figures 12a and 12c). This difference can be caused by the difference in the IDSW formation associated with sea-ice production and timing of its outflow from the formation region to the south.

[33] Table 3 summarizes the average values of the total, MDSW, and IDSW transports. The values at M7 are averaged for fall and winter separately. At M2 and M3 in 1998–1999, the total and MDSW values were comparable, but the IDSW transport for $\sigma_\theta > 26.7$ at M2 was more than twice the value at M3. (The average IDSW ratios were $\sim 33\%$ and 13% at M2 and M3, respectively.) On the other hand, the IDSW transport for $\sigma_\theta > 26.8$ was about 1.5 times

Table 4. Similar to Table 3 Except Only at M2 During Different Periods for Comparison

	1999/9–11	1999/12–2000/3	1998/9–1999/6
Total	2.55	5.13	3.87
MDSW	2.48	4.21	3.04
IDSW	0.92	0.69	1.06
	(0.80)	(0.17)	(0.29)

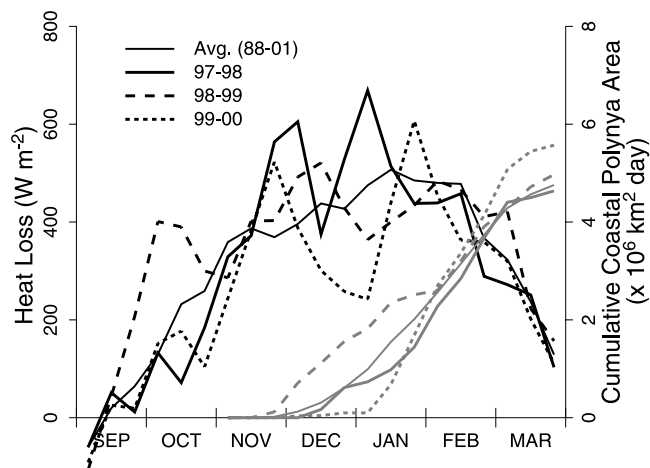


Figure 13. Heat loss from the open water area (black curves) and the cumulative area of coastal polynya (shaded curves) in the region over the northwest shelf (Figure 1) estimated from the heat-budget analysis and SSM/I data, respectively. Plotted values are for three winters before and during the mooring period and the average during 1988–2001.

larger at M2 than at M3. This is partly due to the fact that the higher-density range was not covered well by the instruments in winter at M2 (Figure 6a). For the sake of comparison, the transport at M2 is summarized over different periods in Table 4. All values were much larger at M7 than at the downstream M2 location for the same periods. In September–November 1999, there was considerable difference in the total transport, which mainly caused the differences in the MDSW and IDSW values. (The average IDSW ratios were $\sim 49\%$ and 37% at M7 and M2, respectively.) From December 1999 to March 2000, the total and MDSW values were comparable, but the IDSW value was much larger at M7. In fact, the average IDSW ratios were $\sim 31\%$ and 16% at M7 and M2, respectively. This indicates vigorous mixing between the IDSW and offshore water from M7 and M2. A comparison of transport estimates at M2 between in September–June of 1998–1999 and 1999–2000 gives a measure of interannual variability.

5. Summary and Discussion

[34] Both CTD/XBT and mooring data indicated considerable modification of DSW in the slope region off northern Sakhalin. Vertical sections of temperature and potential density (Figures 3–5) showed significant changes southward from 54.4°N – 55.3°N to 54°N to 53°N . Time series of temperature and potential density in the slope region (Figure 6) also showed considerable warming between the two moorings at 54.9°N and 53°N (M7 and M2), separated by ~ 220 km in the north-south direction (Figures 6c and 6d).

[35] The generation of eddies and associated offshore dense water transport by baroclinic instability over the continental shelf and slope with the application of negative buoyancy forcing have been studied numerically by Kikuchi *et al.* [1999], Gawarkiewicz [2000], and Tanaka and

Akitomo [2001], among others. Over the northwest shelf, Shcherbina *et al.* [2004a] found indications of baroclinic instability of the polynya rim current [Gawarkiewicz and Chapman, 1995] from late February to early May 2000 at their western mooring (see Figure 1 for the location). At M7 (~ 340 km downstream of the mooring on the northwest shelf), the large onshore eddy heat flux suggests the occurrence of baroclinic instability (Table 2). Weaker onshore eddy heat flux farther downstream from M7 suggests that baroclinic instability does not occur far from the DSW source region. Cold anticyclonic eddies were merely advected southward at M3 and M4 along 53°N (Figure 9). The existence of isolated eddies is also suggested in hydrographic sections off northern Sakhalin (Figures 3b, 4a, and 4b).

[36] Cold DSW in the intermediate layer below $26.8\sigma_{\theta}$ was almost entirely absent in the vertical sections south of 51.3°N (Figures 3c, 3d, 4d, and 5d). This absence may be partially explained by the existence of a cyclonic gyre generated by wind stress curl over the northern half of the Okhotsk Sea [Ohshima *et al.*, 2004] because the eastward flowing southern boundary of the gyre is located at $\sim 52^{\circ}\text{N}$. Therefore, in addition to the onshore eddy heat flux, this gyre may be another possible mechanism that can reduce the DSW transport southward along Sakhalin.

[37] Both CTD/XBT and mooring data also indicated large variability in the distribution of DSW over the 3 years. The hydrographic data (Figures 3–5) showed that water in the DSW density range was much colder off the slope in 1999 than in the other 2 years. At mooring M2 at 53°N , where data were obtained in both 1998–1999 and 1999–2000, seasonal variability was quite different in these 2 years (Figures 6a and 6c). These data suggest that the largest DSW production during 1997–2000 occurred during winter 1998–1999.

[38] Assuming isopycnal mixing between the idealized DSW (IDSW) at the freezing point and warm offshore water (Figure 2), the modified DSW (MDSW) transport (Figure 11) calculated from the mooring data is converted to IDSW transport (Figure 12). The resultant IDSW transport shows that it was confined near the shelf break (Figures 12a and 12b), and its seasonal variability differed between 1998–1999 and 1999–2000 (Figures 12a and 12c). This different seasonal variability can be caused by not only the different IDSW volume, but different timing of its outflow from the formation region. During fall 1999, the IDSW transport was largest at M2 and M7 (Figures 12c and 12d). This result supplements the following previous studies. Using hydrographic data on the northern shelves taken in April–October 1997, Gladyshev *et al.* [2000] showed that most DSW left the northwest shelf before July, but DSW existed there even in September due to slow DSW flux during the second half of the year. Also, on the basis of the DSW volumes in May–June and September–October estimated from the historical data, Gladyshev *et al.* [2003] suggested $\sim 30\%$ of DSW in spring remains over the northern shelves in December. The mooring data in this study clearly show the remaining DSW exiting from the northwest shelf even in fall.

[39] Since the IDSW formation is related to sea-ice production, two important factors governing it, heat loss from the open water area and the area of coastal polynya,

are calculated over the northwest shelf (Figure 13). The heat loss is estimated following the heat-budget analysis of Ohshima *et al.* [2003] using bulk parameterizations with various global and objective data sets. In the SSM/I sea-ice data, the coastal polynya area is identified as the thin (new and young) ice area based on the algorithm by Kimura and Wakatsuchi [1999]. Although both CTD/XBT and mooring data indicated that the largest DSW production during 1997–2000 occurred during winter 1998–1999, Figure 13 does not show that the heat loss in this winter was particularly large compared with that in other winters. This shows the difficulty in estimating the DSW production using heat-budget analysis without in situ data [Shcherbina *et al.*, 2003]. However, the polynya area in 1998–1999 was the largest among these winters, and heat loss was the largest during early fall in 1998 among these years. The largest heat loss during early fall in 1998 was consistent with the earlier advent of sea ice at M1 in 1998 than in 1999 (Figures 8a and 8c).

[40] To compare the current DSW transport estimate with those from previous studies (summarized in section 1), the annual mean IDSW volume transport is estimated at 53°N using transport per unit zonal length at M2 and M3. It is calculated for $\sigma_\theta > 26.7$ and a duration of 1 year starting from September 1998. A value between M2 and M3 is derived by linearly interpolating values at M2 and M3. Transport in the triangular region between the slope bottom and M2 is derived by extrapolating values at M2, assuming that they are the same as those at M2. Transport east of M3 is derived by extrapolating linearly with the gradient between M2 and M3 to an offshore zero-crossing point. In the region between M2 and M3, the transport is ~ 0.15 Sv. Adding contributions from the regions west of M2 (~ 0.03 Sv) and east of M3 (~ 0.03 Sv), this value becomes ~ 0.21 Sv.

[41] Although it is not straightforward to compare estimates in this and previous studies, due to different definitions of DSW, the value obtained here is at the lower end of the previous values. There are several possible reasons for this small value. The onshore eddy heat flux observed in the slope regions can reduce the DSW transport at 53°N. The depth range of instruments at M2 was not extensive enough to cover all of the DSW potential density range of 26.7–27.1 σ_θ throughout the mooring period. Owing to the failure of the CT sensor to measure conductivity at M1, DSW over the shelf is not included here. With only two moorings in the slope region, the core of the DSW transport was not likely captured well here. This was most likely the case when little DSW larger than 26.8 σ_θ was observed at M2 in January–February. Although we assume the isopycnal mixing between the IDSW and offshore water here, the IDSW mixing ratio can be significantly reduced if the IDSW is mixed diapycnally with warm water closer to the surface or in the deep ocean. All five of these conditions could result in underestimating the IDSW transport. In conclusion, DSW is not simply carried southward by the ESC but is also diffused offshore by eddy flux off northern Sakhalin.

[42] **Acknowledgments.** We are deeply indebted to Yuri Volkov of Far Eastern Regional Hydrometeorological Institute for making the joint cruises possible. Thanks are extended to the officers, crew and scientists on

board R/V *Professor Khromov* for their help with the field observations. The calibration of the CTD data obtained in 1999 and 2000 was performed by the Oceanographic Data Facility of Scripps Institution of Oceanography. Discussions with Sergey Gladyshev and Motoyo Itoh were helpful. Comments from Seelye Martin and two anonymous reviewers were also helpful. This work was sponsored by the Core Research for Evolutional Science and Technology of Japan Science and Technology Corporation.

References

- Alfulit, M. A., and S. Martin (1987), Satellite passive microwave studies of the Sea of Okhotsk ice cover and its relation to oceanic processes, 1978–1982, *J. Geophys. Res.*, **92**, 13,013–13,028.
- Gawarkiewicz, G. (2000), Effects of ambient stratification and shelfbreak topography on offshore transport of dense water on continental shelves, *J. Geophys. Res.*, **105**, 3307–3324.
- Gawarkiewicz, G., and D. C. Chapman (1995), A numerical study of dense water formation and transport on a shallow, sloping continental shelf, *J. Geophys. Res.*, **100**, 4489–4507.
- Gladyshev, S., S. Martin, S. Riser, and A. Figurkin (2000), Dense water production on the northern Okhotsk shelves: Comparison of ship-based spring-summer observations for 1996 and 1997 with satellite observations, *J. Geophys. Res.*, **105**, 26,281–26,300.
- Gladyshev, S., L. Talley, G. Kantakov, G. Khen, and M. Wakatsuchi (2003), Distribution, formation and seasonal variability of Okhotsk Sea Mode Water, *J. Geophys. Res.*, **108**, 3186, doi:10.1029/2001JC000877.
- Itoh, M., K. I. Ohshima, and M. Wakatsuchi (2003), Distribution and formation of Okhotsk Sea Intermediate Water: An analysis of isopycnal climatology data, *J. Geophys. Res.*, **108**, 3258, doi:10.1029/2002JC001590.
- Kikuchi, T., M. Wakatsuchi, and M. Ikeda (1999), A numerical investigation of the transport process of dense shelf water from a continental shelf to a slope, *J. Geophys. Res.*, **104**, 1197–1210.
- Kimura, N., and M. Wakatsuchi (1999), Processes controlling the advance and retreat of sea ice in the Sea of Okhotsk, *J. Geophys. Res.*, **104**, 11,137–11,150.
- Kitani, K. (1973), An oceanographic study of the Okhotsk Sea—particularly in regard to cold waters, *Bull. Far Seas Fish. Res. Lab.*, **9**, 45–77.
- Martin, S., R. Drucker, and K. Yamashita (1998), The production of ice and dense shelf water in the Okhotsk Sea polynyas, *J. Geophys. Res.*, **103**, 27,771–27,782.
- Mizuta, G., Y. Fukamachi, K. I. Ohshima, and M. Wakatsuchi (2003), Structure and seasonal variability of the East Sakhalin Current, *J. Phys. Oceanogr.*, **33**, 2430–2445.
- Nakatsuka, T., C. Yoshikawa, M. Toda, K. Kawamura, and M. Wakatsuchi (2002), An extremely turbid intermediate water in the Sea of Okhotsk: Implication for the transport of particulate organic matter in a seasonally ice-bound sea, *Geophys. Res. Lett.*, **29**(16), 1757, doi:10.1029/2001GL014029.
- Ohshima, K. I., M. Wakatsuchi, Y. Fukamachi, and G. Mizuta (2002), Near-surface circulation and tidal currents of the Okhotsk Sea observed with the satellite-tracked drifters, *J. Geophys. Res.*, **107**(C11), 3195, doi:10.1029/2001JC001005.
- Ohshima, K. I., T. Watanabe, and S. Nihashi (2003), Surface heat budget of the Sea of Okhotsk during 1987–2001 and the role of sea ice on it, *J. Meteorol. Soc. Jpn.*, **81**, 653–677.
- Ohshima, K. I., D. Simizu, M. Itoh, G. Mizuta, Y. Fukamachi, S. C. Riser, and M. Wakatsuchi (2004), Sverdrup balance and the cyclonic gyre in the Sea of Okhotsk, *J. Phys. Oceanogr.*, **34**, 513–525.
- Shcherbina, A. Y., L. D. Talley, and D. L. Rudnick (2003), Direct observations of North Pacific ventilation: Brine rejection in the Okhotsk Sea, *Science*, **302**, 1952–1955.
- Shcherbina, A. Y., L. D. Talley, and D. L. Rudnick (2004a), Dense water formation on the northwestern shelf of the Okhotsk Sea: I. Direct observations of brine rejection, *J. Geophys. Res.*, **109**, C09S08, doi:10.1029/2003JC002196, in press.
- Shcherbina, A. Y., L. D. Talley, and D. L. Rudnick (2004b), Dense water formation on the northwestern shelf of the Okhotsk Sea: II. Quantifying the transports, *J. Geophys. Res.*, **109**, C09S09, doi:10.1029/2003JC002197, in press.
- Talley, L. D. (1991), An Okhotsk Sea water anomaly: Implications for ventilation in the North Pacific, *Deep Sea Res.*, **38**, Suppl. 1, 171–190.
- Tanaka, K., and K. Akitomo (2001), Baroclinic instability of density current along a sloping bottom and the associated transport process, *J. Geophys. Res.*, **106**, 2621–2638.
- Thompson, R. O. R. Y. (1983), Low-pass filters to suppress inertial and tidal frequencies, *J. Phys. Oceanogr.*, **13**, 1077–1083.
- Warner, M. J., J. L. Bullister, D. P. Wisegarver, R. H. Gammon, and R. F. Weiss (1996), Basin-wide distributions of chlorofluorocarbons

- F-11 and F-12 in the North Pacific, *J. Geophys. Res.*, *101*, 20,525–20,542.
- Wong, C. S., R. G. Matear, H. J. Freeland, F. A. Whitney, and A. S. Buchkov (1998), WOCE line P1W in the Sea of Okhotsk: 2. CFCs and the formation rate of intermediate water, *J. Geophys. Res.*, *103*, 15,625–15,642.
- Yamamoto, M., S. Watanabe, S. Tsunogai, and M. Wakatsuchi (2002), Effects of sea ice formation and diapycnal mixing on the Okhotsk Sea intermediate water clarified with oxygen isotopes, *Deep Sea Res., Part I*, *49*, 1165–1174.
- Yamamoto, M., S. Watanabe, S. Tsunogai, and M. Wakatsuchi (2004), Chlorofluorocarbons in the Okhotsk Sea: Ventilation of intermediate water, *J. Geophys. Res.*, *109*, C09S11, doi:10.1029/2003JC001919, in press.
- Yasuda, I. (1997), The origin of the North Pacific Intermediate Water, *J. Geophys. Res.*, *102*, 893–909.
-
- Y. Fukamachi, K. I. Ohshima, and M. Wakatsuchi, Institute of Low Temperature Science, Hokkaido University, Sapporo 060-0819, Japan. (yasuf@lowtem.hokudai.ac.jp)
- G. Mizuta, Graduate School of Environmental Earth Science, Hokkaido University, Sapporo 060-0810, Japan. (mizuta@ees.hokudai.ac.jp)
- S. C. Riser, School of Oceanography, University of Washington, Seattle, WA 98195, USA. (riser@ocean.washington.edu)
- L. D. Talley, Scripps Institution of Oceanography, University of California, San Diego, La Jolla, CA 92075, USA. (lynne@gyre.ucsd.edu)